nature neuroscience

A crosstalk between β1 and β3 integrins controls glycine receptor and gephyrin trafficking at synapses

Cécile Charrier[1], Patricia Machado[1], Ry Y Tweedie-Cullen[2], Dorothea Rutishauser[3], Isabelle M Mansuy[2] & Antoine Triller[1]

The regulation of glycine receptor (GlyR) number at synapses is necessary for the efficacy of inhibition and the control of neuronal excitability in the spinal cord. GlyR accumulation at synapses depends on the scaffolding molecule gephyrin and is linked to GlyR synaptic dwell time. However, the mechanisms that tune GlyR synaptic exchanges in response to different neuronal environments are unknown. Integrins are cell adhesion molecules and signaling receptors. Using single quantum dot imaging and fluorescence recovery after photobleaching, we found in rats that β1 and β3 integrins adjust synaptic strength by regulating the synaptic dwell time of both GlyRs and gephyrin. β1 and β3 integrins crosstalked via calcium/calmodulin-dependent protein kinase II and adapted GlyR lateral diffusion and gephyrin-dependent trapping at synapses. This provides a mechanism for maintaining or adjusting the steady state of postsynaptic molecule exchanges and the level of glycinergic inhibition in response to neuron- and glia-derived signals or extracellular matrix remodeling.

Although synapses are relatively stable structures, their molecular components are exchanged on short time scales[1]. Postsynaptic scaffolding molecules are renewed in tens of minutes both *in vitro* and *in vivo* (for example, see refs. 2–4). In the neuronal membrane, recent advances in single particle imaging techniques have enabled the visualization of neurotransmitter receptor lateral diffusion into and out of synapses[1,5]. As receptors are mostly inserted in and removed from the plasma membrane at nonsynaptic sites[1], lateral diffusion and trapping at synapses are fundamental mechanisms for the sorting and accumulation of receptors at excitatory or inhibitory synapses. Synaptic strength is closely related to the dwell time of the postsynaptic molecules and both can be adjusted during synapse maturation and plasticity[1,3]. However, the manner in which changes in the neuronal environment are translated into changes in the dwell times of synaptic molecules remains unknown.

Integrins mediate adhesion between the extracellular matrix (ECM) and the cytoskeleton and transduce bidirectional signaling cascades[6,7]. They are transmembrane heterodimers composed of one α and one β subunit, which are receptors for ECM molecules, soluble factors and counter-receptors. At least ten integrin subunits are expressed in the CNS[8] and some are localized at synapses (for example, see refs. 8–11). Integrins are central elements in neuron-neuron and neuron-glia interactions during synapse maturation, synapse plasticity, and after injury[10,12,13]. Recent studies have found that β1 and β3 integrins are involved at excitatory synapses. In hippocampal neurons, β1 integrins are required for long-term potentiation and spatial memory[9,14–16]. β3 integrins coordinate the maturation of the pre- and postsynaptic compartments and mediate activity-dependent regulation of excitatory synaptic strength[10,11]. The function of integrins at inhibitory synapses remains unknown.

We investigated the function of β1 and β3 integrins at glycinergic synapses in spinal cord neurons. GlyRs are important for controlling motor neuron excitability and processing sensory signals[17]. We focused our attention on GlyRs containing the α1 subunit, which predominate in the adult spinal cord[17]. These receptors are α1/β hetero-pentamers and are stabilized at synapses by direct interaction between the β subunit and gephyrin, the main inhibitory scaffolding protein[4]. We found that β1 and β3 integrins adjusted glycinergic synaptic strength in an opposing manner: β1 integrins increased GlyR numbers at synapses and β3 integrins reduced GlyR numbers and glycinergic synaptic strength. Using single molecule and bulk approaches, we found that these effects result from a regulation of both gephyrin exchange and GlyR dwell time at synapses. The opposing actions of β1 and β3 integrins rely on calcium/calmodulin-dependent protein kinase II (CaMKII), which regulates GlyR trapping and accumulation at synapses. We also found that β1 and β3 integrins can be further activated by extracellular factors, such as thrombospondin 1 (TSP1) and fibrinogen, that are released after injury. Thus, the crosstalk between β1 and β3 integrins provides a mechanism for the regulation of glycinergic synaptic strength integrating signals from neurons and glia.

RESULTS

Opposite actions of β1 and β3 integrins on synaptic GlyRs

To test the possible involvement of integrins at glycinergic synapses, we blocked integrin function in cultured spinal cord neurons using echistatin, a peptide from viper venom, which contains an arginine-glycine-aspartate (RGD) motif that specifically inhibits integrins containing the β1 and β3 subunits[18]. We analyzed the effects of 1-h treatment with echistatin (100 nM) on GlyR synaptic clusters using

[1]Biologie Cellulaire de la Synapse, IBENS, Ecole Normale Supérieure, Inserm U1024, CNRS UMR8197, Paris, France. [2]Brain Research Institute, University of Zürich, Swiss Federal Institute of Technology, Zürich, Switzerland. [3]Functional Genomics Center Zürich, University of Zürich, Swiss Federal Institute of Technology, CH-8057 Zürich, Switzerland. Correspondence should be addressed to A.T. (triller@biologie.ens.fr).

Received 24 March; accepted 26 August; published online 10 October 2010; doi:10.1038/nn.2645

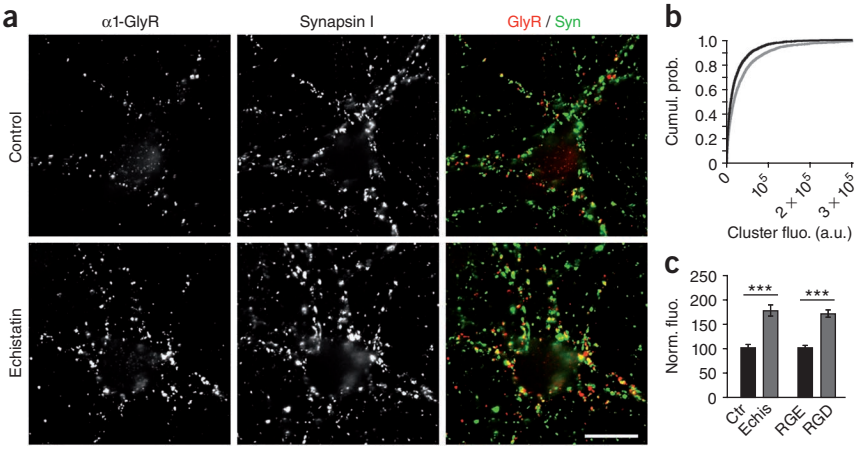

Figure 1 RGD peptides increase GlyR numbers at synapses. (**a**) Spinal cord neurons (12 d *in vitro*) stained for α1-GlyR and synapsin I in control conditions or after treatment with echistatin (1 h, 100 nM). Scale bar represents 20 μm. (**b**) Cumulative probability plot of synaptic GlyR cluster–associated fluorescence in control conditions (black) and after a 1-h echistatin treatment (gray) (control, $n = 2{,}740$; echistatin, n = 2,549; from 21 cells by condition, $P < 0.001$, Mann-Whitney test). a.u., arbitrary unit. (**c**) Increased GlyR-associated fluorescence intensity at synapses after treatment with echistatin or GRGDSP peptide (gray) compared with control or treatment with GRGESP peptide (black). Ctr, control; Echis, ehcistatin; RGE, GRGESP; RGD, GRGDSP Mean ± s.e.m. (***$P < 0.001$, *t* test).

synapsin I to identify synapses. After echistatin treatment, GlyR clusters were brighter than those in control conditions (**Fig. 1a**,**b**). GlyR immunoreactivity at synapses increased to 177 ± 11% of the control (control, $n = 52$; echistatin, $n = 51$; $P < 0.001$; **Fig. 1c**). Similar results were obtained with a synthetic RGD peptide (GRGESP, $n = 54$; GRGDSP, $n = 54$; $P < 0.001$; **Fig. 1c**). These findings indicate that integrins control GlyR accumulation at synapses.

To discriminate between the effects of β1 and β3 integrins on GlyR clusters, we used monoclonal antibodies that specifically block β1 or β3 integrins. A 1-h treatment with β3-blocking antibodies (aβ3, 25 μg ml^{-1}) increased GlyR cluster immunoreactivity to 198 ± 11% of the control (control, $n = 60$; aβ3, $n = 60$; $P < 0.001$; **Fig. 2a**,**b**). In contrast, treatment with β1-blocking antibodies (aβ1, 25 μg ml^{-1}) reduced GlyR cluster immunoreactivity to 57 ± 2% of the control (control, $n = 60$; aβ1, $n = 60$; $P < 0.001$). The difference between the effects of RGD peptides and those of aβ1 can be explained by the fact that, depending on the α subunit, some αβ1 heterodimers are not receptors for RGD-containing molecules[6] and are therefore not inhibited by these peptides. A 1-h treatment with aβ1 or aβ3 had no effect on synapse density or on synapse size (**Supplementary Fig. 1**). Consistent with this, the robust changes in GlyR cluster immunoreactivity after aβ1 and aβ3 treatments were not associated with similar modifications of GlyR cluster size (**Supplementary Fig. 1**). This is consistent with previous reports on synapse number or morphology[11,14,15,19].

To further substantiate the opposite effects of the β1 and β3 integrin blocking antibodies, we overexpressed truncated forms of β1 and β3 integrins (CTβ1 and CTβ3, respectively[11]) in which the extracellular domain was replaced by enhanced green fluorescent protein (EGFP). The low transfection efficiency allowed us to analyze the effects of postsynaptic integrin blockade by examining transfected postsynaptic neurons that were not surrounded by transfected axons. After 24 h, overexpression of CTβ3 resulted in a robust increase in receptor cluster–associated fluorescence (206 ± 23% of the control), whereas overexpression of CTβ1 had the opposite effect (55 ± 4% of the control; EGFP, $n = 37$; CTβ1, $n = 40$; CTβ3, $n = 38$; $P < 0.001$; **Supplementary Fig. 2**). The direction and the amplitude of these changes were similar to those observed after 1-h treatment with the blocking antibodies. Together, these results suggest that β1 and β3 integrins regulate GlyR numbers at synapses in an opposing manner.

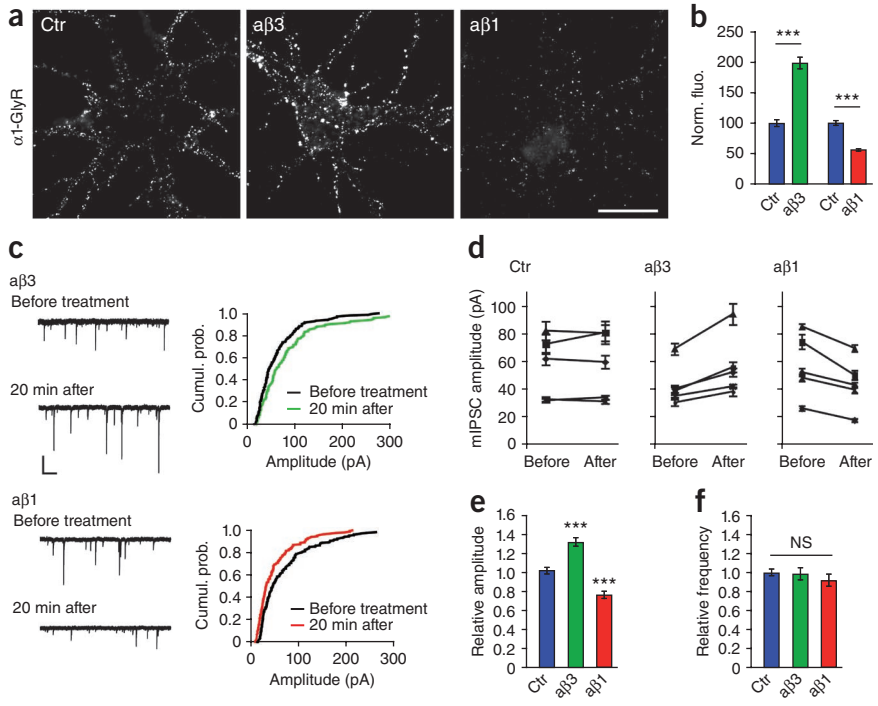

Figure 2 β1 and β3 integrin blocking antibodies have opposite effects on GlyR numbers at synapses. (**a**) Nonpermeabilized cells stained for α1-GlyR in control conditions or after 1-h treatment with β3 (aβ3) or β1 (aβ1) function-blocking antibodies. Scale bar represents 20 μm. (**b**) Normalized fluorescence intensity associated with GlyR clusters (mean ± s.e.m., ***$P < 0.001$, *t* test). (**c**) Examples of glycinergic mIPSCs and cumulative probability plot of their amplitudes from 2-min recording periods from the same cells before and 20 min after aβ3 or aβ1 treatment. Scale bars represent 100 pA and 1 s. (**d**) Average mIPSC amplitude before and after aβ1 or aβ3 treatment or after a 20-min time lag (control) for each cell (control, not significant (NS), $P > 0.05$; aβ1 and aβ3, $P < 0.01$; Mann-Whitney test). (**e**) Relative effects on mIPSC amplitudes. Mean amplitudes after treatment are plotted relative to the mean amplitudes before treatment (***$P < 0.001$, ANOVA). (**f**) Mean effects on mIPSC frequency ($P > 0.05$, ANOVA). Error bars indicate s.e.m.

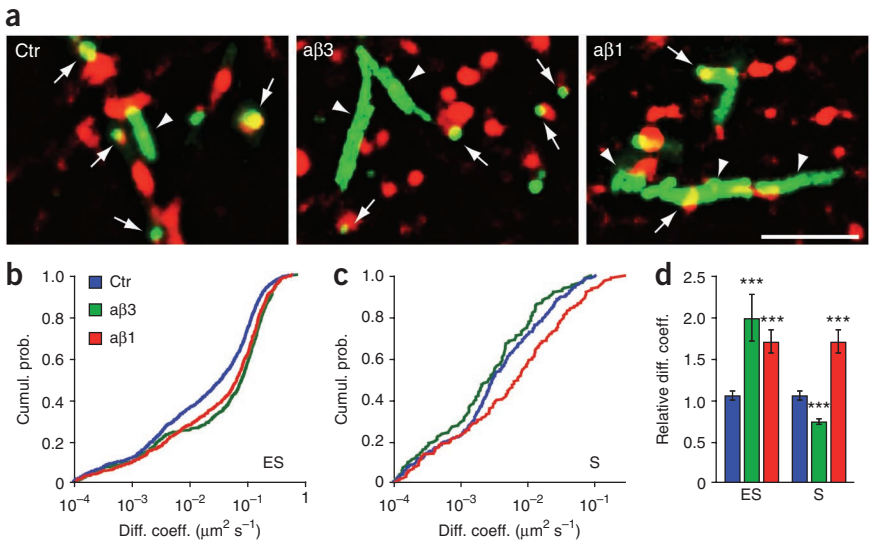

Figure 3 β1 and β3 integrins control GlyR lateral diffusion. (**a**) Maximum intensity projections of 512 frames recorded at 13 Hz for 38.4 s. The GlyR-QD traces and FM4-64–stained synapses are green and red, respectively; yellow denotes their overlap. The GyR-QD–explored area increased after aβ3 or aβ1 treatment in the extrasynaptic membrane (arrowheads). At synapses, aβ3 and aβ1 reduced and increased GlyR-QD mobility (arrows), respectively. Scale bar represents 5 μm. (**b**) Cumulative probability plot of GlyR-QD diffusion coefficients in the extrasynaptic membrane (ES, $P < 0.001$, Mann-Whitney test). (**c**) Cumulative probability plot of GlyR-QD diffusion coefficients at synapses (S: aβ3, $P < 0.01$; aβ1, $P < 0.001$; Mann-Whitney test). (**d**) Normalized effects of aβ1 and aβ3 on GlyR-QD diffusion coefficients (mean ± s.e.m., $^{***}P < 0.001$, ANOVA). Control values indicate the relative fluctuation between two control distributions (Ctra and Ctrb) of diffusion coefficients (ES: $n_{Ctra} = 300$, $n_{Ctrb} = 524$; S: $n_{Ctra} = 300$, $n_{Ctrb} = 524$). Note that β1 and β3 integrin inhibition had comparable effects in the extrasynaptic membrane and opposite effects at synapses.

The functional consequences of the regulation of GlyR numbers at synapses were tested with whole-cell patch-clamp recordings. We compared miniature glycinergic postsynaptic currents (mIPSCs) from the same cells before and after antibody application. mIPSC amplitudes were increased after β3 integrin inhibition and were reduced after β1 integrin inhibition (**Fig. 2c**,**d**), consistent with the effects observed with immunocytochemistry. By 20 min after aβ3 application, mIPSC amplitudes were increased to 132 ± 4% of the amplitudes before treatment, whereas they were decreased to 76 ± 4% after aβ1 application ($n = 5$ for each condition, $P < 0.001$; **Fig. 2e**). The coefficient of variation of the mIPSC amplitudes was not modified after aβ1 or aβ3 treatment (**Supplementary Fig. 3**), indicating that β1 and β3 integrins uniformly scale the synaptic strength of all glycinergic synapses. Moreover, the kinetics of the mIPSCs remained unchanged (**Supplementary Fig. 3**). The frequency of the mIPSCs varied between cells from 1.0 ± 0.4 Hz to 7.5 ± 0.3 Hz, but was not modified by aβ1 and aβ3 treatments ($P > 0.05$; **Fig. 2f**). The effects of aβ3 and aβ1 treatments were not observed with denatured antibodies (data not shown). These data indicate that β1 and β3 integrins scale inhibitory synaptic strength in opposite directions by modifying GlyR number at synapses.

Integrins control GlyR lateral diffusion

We previously found that GlyR diffusion trapping is important for the regulation of GlyR number at synapses[5,20,21]. To test the effects of integrin inhibition on GlyR diffusion properties in the neuronal membrane, we stained active presynaptic boutons with FM4-64 and monitored the surface mobility of endogenous GlyRs labeled with quantum dots (GlyR-QDs) in single particle tracking (SPT) experiments. The SPT method provides a high spatial resolution (~10 nm)[5]. Consistent with previous observations[5,20], some GlyR-QDs remained at synapses or diffused in the extrasynaptic membrane, whereas others entered or escaped the synaptic area during the recording session (**Fig. 3a**). After aβ3 treatment, GlyR-QDs generally explored larger surfaces of the extrasynaptic membrane, but smaller surfaces at synapses. After aβ1 treatment, GlyR-QDs were very mobile in and outside synapses and were frequently exchanged between the synaptic and extrasynaptic compartments.

Quantification of these experiments indicated that, in the extrasynaptic membrane, GlyR-QD diffusion coefficients were about twofold larger than control values after both aβ3 and aβ1 treatments (control, $n = 1{,}112$; aβ3, $n = 626$; aβ1, $n = 682$; $P < 0.001$; **Fig. 3b**). At synapses, however, β3 and β1 integrin blockade had opposite effects: GlyR-QD diffusion coefficients were decreased after aβ3 treatment (control, $n = 288$; aβ3, $n = 152$; $P < 0.01$), whereas they were increased after aβ1 treatment (aβ1, $n = 176$, $P < 0.001$; **Fig. 3c**). The diffusion coefficients were decreased to 75% of the control after β3 integrin inhibition and increased to 170% of the control after β1 integrin inhibition (**Fig. 3d**). Thus, the effects of β1 and β3 integrin inhibition are comparable at the extrasynaptic membrane, but opposite at synapses, indicating that there is distinct regulation in the two compartments.

Integrins control GlyR trapping and dwell time at synapses

Given the effects on GlyR diffusion at synapses, we hypothesized that integrins regulate the level of confinement of synaptic receptors. We analyzed the trajectories of GlyR-QDs in more detail (**Fig. 4a**). As shown by plots of the mean square displacement (MSD), GlyRs were more confined after β3 integrin inhibition, but less confined after β1 integrin inhibition (**Fig. 4b**). In control conditions, the average diameter of the confinement domain at synapses was 175 ± 9 nm ($n = 228$ trajectories), which is consistent with previous data[20]. The size of the confinement domain was reduced to 71 ± 5% of the control after β3 integrin inhibition, whereas it was enlarged to 150 ± 10% of the control after β1 integrin inhibition (aβ3, $n = 115$; aβ1, $n = 124$; $P < 0.001$; **Fig. 4c**). This indicates that β1 integrin inhibition induces a relaxation of the constraints that stabilize the GlyRs at synapses and therefore facilitates GlyR exit from synapses, whereas β3 integrin inhibition has an opposing action.

We then tested whether the changes in GlyR confinement affected the time spent by GlyRs at synapses when they diffuse in the plasma membrane. Receptor dwell time in a synapse may vary between seconds and tens of minutes[5], which exceeds the duration of our recordings (38.4 s). We therefore used a dwell time index to estimate the mean fraction of time spent in a synapse (see Online Methods). The cumulative distribution of this index highlighted two populations

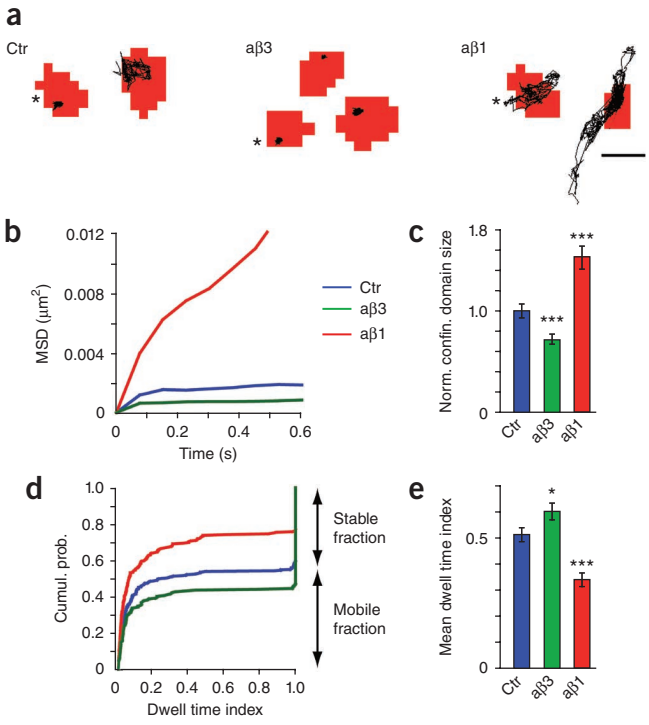

Figure 4 β1 and β3 integrins modulate GlyR confinement and dwell time at synapses. (**a**) Examples of GlyR-QD trajectories (black) over FM4-64–stained synapses (red) from control, aβ3- and aβ1-treated neurons. Trajectories analyzed in **b** are denoted with an asterisk. Scale bar represents 1 μm. (**b**,**c**) Treatment with aβ3 (green) and aβ1 (red) increased and decreased confinement of GlyR-QDs, respectively. MSD versus time plot for GlyR-QD trajectories indicated in **a** is shown in **b**. The normalized size of the confinement domain at synapses is shown in **c**. Note that the smaller the confinement domain, the greater the confinement (mean ± s.e.m., $***P < 0.001$, Mann-Whitney test). (**d**,**e**) Dwell time of GlyR-QDs at synapses. A cumulative probability plot (**d**) and mean dwell time index (**e**) are shown. Error bars indicate s.e.m. ($*P < 0.05$, Mann-Whitney test).

of receptors (**Fig. 4d**): a 'stable' population, corresponding to receptors that were always detected at synapses during the recording session (dwell time index = 1), and a 'mobile' population, corresponding to receptors that were exchanged between the synaptic and extrasynaptic compartments (dwell time index < 1). β1 integrin inhibition reduced GlyR-QD dwell time index from 0.51 ± 0.02 in the control condition to 0.34 ± 0.03, whereas β3 integrin inhibition increased it to 0.60 ± 0.03 (control, $n = 377$; aβ3, $n = 205$, $P < 0.05$; aβ1, $n = 253$, $P < 0.001$; **Fig. 4e**). Thus, GlyRs spent more time at synapses after β3 integrin inhibition and more time in the extrasynaptic membrane after β1 integrin inhibition. Furthermore, we found that integrin-mediated regulation of GlyRs did not depend on GlyR endocytosis, exocytosis, protein synthesis or protein degradation (**Supplementary Fig. 4**), which contrasts with what has been observed for GluR2-containing AMPA receptors[11] (**Supplementary Fig. 4**). Together, these data indicate that β1 and β3 integrins set the equilibrium between the pools of synaptic and extrasynaptic GlyRs and thereby regulate the number of GlyRs at synapses.

Integrins regulate gephyrin stabilization at synapses

At synapses, GlyRs are transiently stabilized by the gephyrin-based postsynaptic scaffold[4]. We tested whether changes in gephyrin assembly were associated with the regulation of GlyR trapping at synapses. Using immunocytochemistry, we found that gephyrin cluster immunoreactivity increased to 161 ± 5% of the control value after aβ3 treatment (control, $n = 60$; aβ3, $n = 60$; $P < 0.001$), whereas it decreased to 59 ± 3% of the control after aβ1 treatment (aβ1, $n = 60$, $P < 0.001$; **Fig. 5a**,**b**), indicating that integrins control the level of gephyrin at synapses. These effects were not associated with modification of gephyrin expression and did not depend on protein synthesis or protein degradation (**Supplementary Fig. 5**), indicating that integrins control the exchange between synaptic and nonsynaptic gephyrin molecules.

To examine the effects of β1 and β3 integrin blockade on the synaptic dynamics of gephyrin, we transfected neurons with a gephyrin-Venus construct (VeGe[22]) and performed fluorescence recovery after photobleaching (FRAP) of individual synaptic VeGe clusters (**Fig. 5c**,**d**). Over a 20-min timescale, the recovery curves exhibited two main phases: a 'fast' component, which corresponds to a population of molecules exchanged in a few seconds with nonsynaptic nonbleached molecules, and a 'slow' component, which corresponds to a population of molecules that could reside in a cluster for tens of minutes (**Fig. 5e**). Integrin inhibition had a noticeable effect on the fast phase of the recovery, which was more rapid and reached a higher plateau after β1 integrin inhibition, but was reduced after β3 integrin inhibition. In contrast, the slow phase was not markedly altered. The fluorescence recovery was 50 ± 2% of the initial value in control condition 10 min after photobleaching ($n = 26$, **Fig. 5f**), which is similar to the recovery obtained

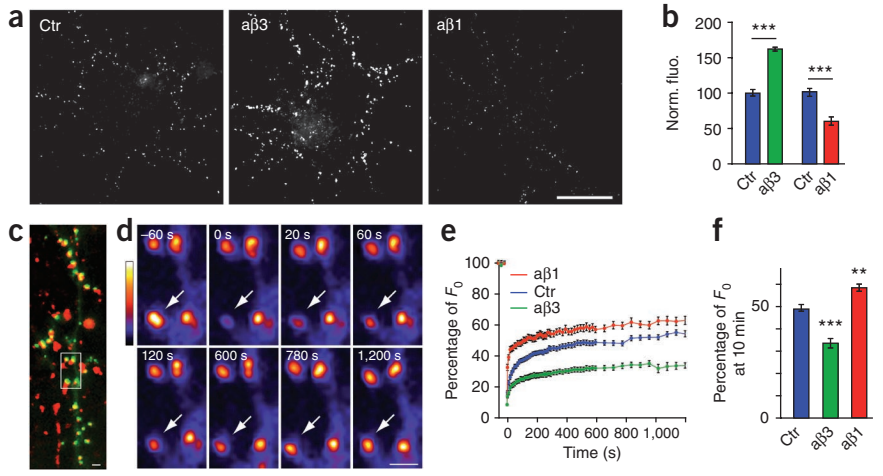

Figure 5 β1 and β3 integrins control gephyrin amount and exchanges at synapses. (**a**) Immunostaining for gephyrin in control conditions or after aβ3 or aβ1 treatment. Scale bar represents 20 μm. (**b**) Normalized fluorescence intensity associated with endogenous gephyrin clusters (mean ± s.e.m., $***P < 0.001$, *t* test). (**c**) Representative example of transfected neurons expressing VeGe (green). VeGe forms clusters in front of active presynaptic boutons stained with FM4-64 (red). The white square outlines the region shown in **d**. Scale bar represents 1 μm. (**d**) Photobleaching of an individual synaptic VeGe cluster (arrow) and time-lapse recording of the fluorescence recovery over 20 min. The color scale indicates the level of fluorescence. (**e**) Fluorescence recovery curves (mean ± s.e.m.). (**f**) Mean fluorescence recovery 10 min after photobleaching (error bars represent s.e.m., $**P < 0.01$ and $***P < 0.001$, Mann-Whitney test). F_0, initial fluorescence.

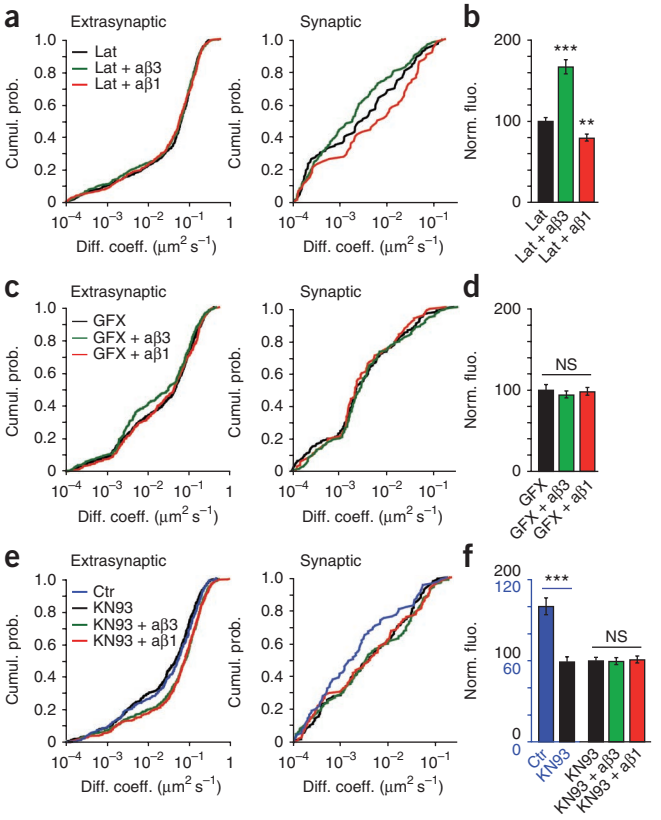

Figure 6 Actin, PKC and CaMKII mediate integrin-dependent regulation of GlyR lateral dynamics. (**a**,**c**,**e**) Cumulative distributions of GlyR-QD diffusion coefficients. (**b**,**d**,**f**) Histograms of normalized fluorescence intensity associated with GlyR clusters (mean ± s.e.m.). (**a**,**b**) Effects of aβ1 (red) and aβ3 (green) treatment after F-actin disruption with latrunculin (Lat, 3 μM, black). Latrunculin abolished the extrasynaptic ($P > 0.05$, Mann-Whitney test), but not the synaptic, effects on GlyR diffusion (Lat and ab1, $P < 0.05$; Lat and ab3, $P < 0.001$, Mann-Whitney test) and cluster immunoreactivity. (**c**,**d**) Effects of aβ1 (red) and aβ3 (green) treatment after PKC inhibition (GFX, 50 nM, black). GFX abolished both the extrasynaptic and synaptic effects on GlyR diffusion ($P > 0.05$, Mann-Whitney test) and cluster immunoreactivity. (**e**,**f**) Effects of CaMKII inhibition (KN-93, 10 μM, black) compared with the control (blue) and effects of aβ1 (red) and aβ3 (green) treatment after CaMKII inhibition. (**e**) In the extrasynaptic membrane, KN-93 had no effect on GlyR mobility. At synapses, KN-93 increased GlyR mobility ($P < 0.001$, Mann-Whitney test) and prevented the effects of aβ1 and aβ3 ($P > 0.05$, Mann-Whitney test). (**f**) At synapses, CaMKII inhibition decreased GlyR cluster immunoreactivity (blue scale, left) and prevented the effects of aβ1 and aβ3 treatments (black scale, right). ***$P < 0.001$ and **$P < 0.01$, NS indicates $P > 0.05$, ANOVA.

with endogenous red fluorescent protein–gephyrin clusters from a knockin mouse[2]. It was increased to 58 ± 2% of the initial value after β1 integrin inhibition ($n = 21$, $P < 0.01$) and reduced to 33 ± 1% after β3 integrin inhibition ($n = 21$, $P < 0.001$). These findings suggest that integrins determine the steady state of gephyrin synaptic exchange. Altogether, our data indicate that the modulation of gephyrin synaptic turnover by β1 and β3 integrins controls the dwell time and the number of GlyRs at synapses.

Integrins control GlyR synaptic trapping via CaMKII

In contrast with other adhesion molecules, such as cadherins and neuroligins, there is no known direct interaction between integrins and postsynaptic proteins. Nonetheless, integrins interact with a number of cytoskeleton-related molecules and signaling proteins[7] that might regulate the interactions in the postsynaptic scaffold. We previously found that F-actin disruption increases GlyR lateral diffusion and reduces the amount of both GlyRs and gephyrin at synapses[20]. We therefore investigated the involvement of the actin cytoskeleton in integrin-mediated regulations of GlyR lateral diffusion. We found that F-actin disruption with latrunculin (3 μM, 25 min) abolished the effect of β1 and β3 integrin inhibition in the extrasynaptic membrane (latrunculin, $n = 484$; latrunculin and aβ3, $n = 621$; latrunculin and aβ1, $n = 386$; $P > 0.05$; **Fig. 6a**). At synapses, however, latrunculin did not prevent the aβ1-induced increase or the aβ3-induced decrease in GlyR diffusion coefficients (latrunculin, $n = 103$; latrunculin and aβ3, $n = 185$, $P < 0.001$; latrunculin and aβ1, $n = 73$, $P < 0.05$). The effects on GlyR clusters were also maintained after latrunculin treatment. β3 integrin blockade increased GlyR cluster immunoreactivity to 167 ± 9%, whereas β1 integrin blockade reduced it to 77 ± 4% of latrunculin values (latrunculin, $n = 40$; latrunculin and aβ3, $n = 40$, $P < 0.001$; latrunculin and aβ1, $n = 40$, $P < 0.01$; **Fig. 6b**). This indicates that the lateral mobility of GlyRs depends on actin in the extrasynaptic membrane, whereas integrins regulate GlyR trapping at synapses via a distinct pathway.

We then examined several kinases involved in integrin signaling. Inhibition of Src kinases did not block the effect of aβ1 or aβ3 on GlyR cluster immunoreactivity (**Supplementary Fig. 6**), suggesting that Src kinases do not contribute to these regulations. Protein kinase C (PKC) inhibition with GF109203X (GFX, 50 nM, 25 min) alone did not modify GlyR lateral diffusion or GlyR accumulation at synapses (**Supplementary Fig. 7**). However, PKC inhibition prevented the effects of integrin inhibition on the lateral diffusion of GlyRs in the extrasynaptic membrane (GFX, $n = 675$; GFX and aβ3, $n = 321$; GFX and aβ1, $n = 353$; $P > 0.05$; **Fig. 6c**) and at synapses (GFX, $n = 230$; GFX and aβ3, $n = 168$; GFX and aβ1, $n = 218$; $P > 0.05$). PKC inhibition also abolished the aβ3-induced increase and the aβ1-induced decrease in the number of GlyRs at synapses (GFX, 100 ± 6%, $n = 40$; GFX and aβ3, 94 ± 4%, $n = 40$; GFX and aβ1, 98 ± 5%, $n = 40$; $P > 0.05$; **Fig. 6d**). Given that integrins regulate GlyR mobility in and out of synapses by different pathways, these results indicate that PKC is necessary for integrin activation, but is not responsible for the synapse-specific antagonism between β1 and β3 integrins.

Next, we tested the involvement of CaMKII. In the extrasynaptic membrane, inhibition of CaMKII with KN-93 (10 μM, 1 h) had no effect on GlyR mobility (control, $n = 279$; KN-93, $n = 505$; $P > 0.05$; **Fig. 6e**) and did not alter the aβ1- and aβ3-induced increase of GlyR diffusion coefficients (KN-93 and aβ3, $n = 489$; KN-93 and aβ1, $n = 450$; $P < 0.001$). At synapses, however, CaMKII inhibition increased GlyR diffusion coefficients (control, $n = 90$; KN-93, $n = 133$; $P < 0.001$) and decreased their synaptic accumulation (control, 100 ± 6%, $n = 40$; KN-93, 59 ± 3%, $n = 40$; $P < 0.001$; **Fig. 6f**). Furthermore, CaMKII inhibition completely abolished the effects of aβ1 and aβ3 on GlyR mobility at synapses (KN-93 and aβ3, $n = 158$; KN-93 and aβ1, $n = 131$; $P > 0.05$; **Fig. 6e**) and on GlyR cluster immunoreactivity (KN-93, 100 ± 4%, $n = 40$; KN-93 and aβ3, 99 ± 4%, $n = 40$; KN-93 and aβ1, 101 ± 4%, $n = 40$; $P > 0.05$; **Fig. 6f**). The effects of aβ1 and aβ3 on gephyrin clusters were also occluded by the CaMKII inhibitor (KN-93, 100 ± 4%, $n = 40$; KN-93 and aβ3, 100 ± 5%, $n = 40$; KN-93 and aβ1, 98 ± 4%, $n = 40$, $P > 0.05$). These results indicate that both β1 and β3 integrins signal via CaMKII, which is responsible for their opposing actions at synapses. Furthermore, these findings demonstrate that controlling GlyR mobility in the synapse is crucial for adjusting the number of synaptic GlyRs.

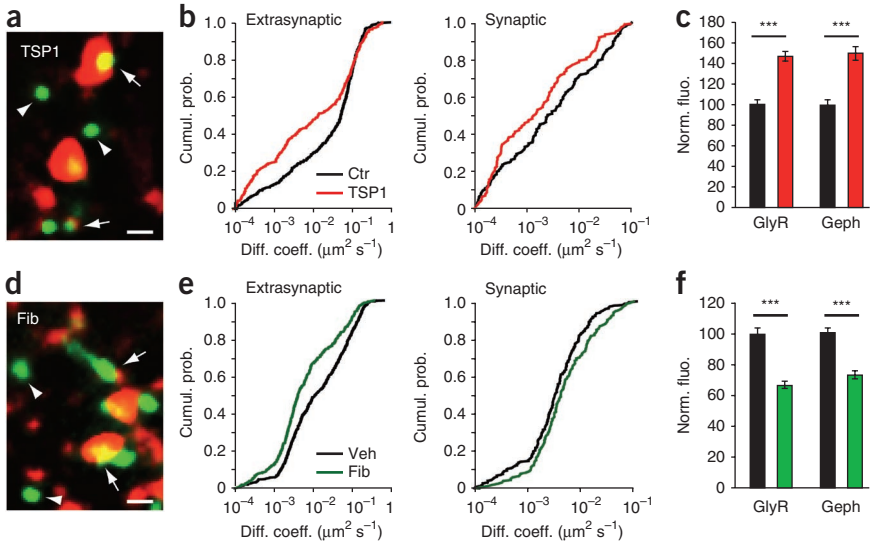

Figure 7 TSP1 and fibrinogen have opposite effects at inhibitory synapses. (**a**) Typical behavior of GlyR-QDs after 1-h treatment with thrombospondin 1 (TSP1, 2 μg ml^{-1}). Maximum intensity projections of 512 frames recorded at 13 Hz. The GlyR-QD explored area is shown in green and FM4-64–stained synapses in red. GlyR-QDs have a reduced mobility in (arrows) and out (arrowheads) of synapses. Scale bar represents 1 μm. (**b**) Distributions of GlyR-QD diffusion coefficients at extrasynaptic and synaptic locations in control condition (black) or after TSP1 treatment (red) ($P < 0.001$, Mann-Whitney test). (**c**) Normalized fluorescence intensity associated with GlyR and gephyrin clusters at synapses (mean ± s.e.m., ***$P < 0.001$, t test). (**d**) Typical behavior of GlyR-QD after 1-h treatment with fibrinogen (Fib, 1.5 mg ml^{-1}). Colors are as described in **a**. GlyR-QDs were very mobile at synapses, but not in the extrasynaptic membrane. (**e**) Distributions of GlyR-QD diffusion coefficients at extrasynaptic and synaptic locations after treatment with fibrinogen (green) or with its vehicle (veh, black) ($P < 0.001$, Mann-Whitney test). (**f**) Data are presented as in **c** (mean ± s.e.m.). Colors are as described in **e**. Note that TSP1 increased the stabilization and the number of GlyRs at synapses, whereas fibrinogen had the opposite effect.

TSP1 and fibrinogen have opposite effects at synapses

Little is known about the ligands of integrins involved in the regulation of synapse function. We examined the effects of TSP1 and fibrinogen, two known β1 and β3 integrin ligands that are released after injury[23–26]. The β1 integrin ligand TSP1 (2 μg ml^{-1}, 1 h) slowed down GlyR lateral diffusion in the extrasynaptic membrane (control, $n = 487$; TSP1, $n = 355$; $P < 0.001$) and stabilized GlyRs at synapses (control, $n = 159$; TSP1, $n = 130$; $P < 0.001$; **Fig. 7a**,**b**). The changes in diffusion properties were associated with an increased accumulation of GlyRs (control, 100 ± 4%, $n = 60$; TSP1, 147 ± 5%, $n = 60$; $P < 0.001$) and gephyrin at synapses (control, 100 ± 4%, $n = 60$; TSP1, 150 ± 6%, $n = 60$; $P < 0.001$; **Fig. 7c**). The effects of TSP1 were opposite to those observed after inhibition of β1 integrins and were abolished by prior incubation with aβ1 (**Supplementary Fig. 8**). These findings indicate that TSP1 increases GlyR trapping through β1 integrins.

The β3 integrin ligand fibrinogen (1.5 mg ml^{-1}, 1 h) slowed GlyR lateral mobility in the extrasynaptic membrane and destabilized GlyRs at synapses (extrasynaptic: vehicle, $n = 614$; fibrinogen, $n = 413$; $P < 0.001$; synaptic: vehicle, $n = 218$; fibrinogen, $n = 152$; $P < 0.001$; **Fig. 7d**,**e**). Consistent with this, fibrinogen decreased GlyR and gephyrin synaptic levels to 67 ± 2% and 73 ± 2% of the control values, respectively (vehicle, $n = 60$; fibrinogen, $n = 60$; $P < 0.001$ for both GlyR and gephyrin; **Fig. 7f**). The effects of fibrinogen were opposite to those observed after inhibition of β3 integrins and were abolished by prior incubation with aβ3 (**Supplementary Fig. 8**), indicating that fibrinogen decreases GlyR trapping via β3 integrins. Taken together, these results strongly suggest that GlyR diffusion trapping and numbers at synapses can be regulated by extracellular factors released after injury.

DISCUSSION

We found that integrins control glycinergic synaptic strength by regulating the number of GlyRs at synapses. Using SPT with blocking antibodies and known integrin ligands, we found that β1 integrins decreased GlyR diffusion coefficients and increased GlyR confinement at synapses, whereas β3 integrins had opposing actions. β1 and β3 integrins adjusted GlyR dwell time at synapses and shifted the equilibrium between the pools of synaptic and extrasynaptic receptors toward an increased and decreased synaptic localization, respectively. Notably, blocking the effects of integrins on GlyR diffusive properties at synapses abolished the regulation of GlyR postsynaptic accumulation. Furthermore, the effects of integrins were not associated with modification of GlyR surface expression and did not depend on endocytosis, protein synthesis or protein degradation. Together, these data reveal that β1 and β3 integrins control GlyR synaptic trapping and residence time, which determine the number of GlyRs at synapses in spinal cord neurons.

It is now well accepted that GlyRs may be associated with gephyrin along the secretion pathway[27] and that a large proportion of GlyRs diffuse into and out of synapses in association with gephyrin[2,28]. This implies that GlyRs can be trapped at synapses by GlyR/gephyrin or gephyrin-gephyrin interactions. Consequently, modulating gephyrin oligomerization is expected to affect the stabilization of both GlyRs and gephyrin molecules at synapses. Consistent with this, it has been shown that overexpression of gephyrin variants with altered oligomerization properties affects GlyR lateral diffusion and postsynaptic accumulation[2,29]. Alternatively, modulating the GlyR/gephyrin interaction may affect GlyR synaptic trapping. It has been shown that gephyrin's interaction with its partner Pin1 regulates GlyR/gephyrin binding[30]. Modifications in the gephyrin-binding sequence of the GlyR β subunit have also been proposed to affect GlyR synaptic localization during activity-dependent homeostatic regulation of glycinergic synapses[21]. To date, the modulation of GlyR/gephyrin interaction has not been associated with changes in postsynaptic accumulation of gephyrin[21,30]. The results of our immunocytochemistry and FRAP experiments suggest that β1 and β3 integrin inhibition modify both the amount of synaptic gephyrin and the exchange between synaptic and nonsynaptic gephyrin molecules. This indicates that β1 and β3 integrins modulate gephyrin oligomerization properties. The regulation of gephyrin oligomerization alone can account for the effects on GlyR and gephyrin dynamics because GlyRs and gephyrin may traffic together and because gephyrin provides the binding sites for GlyRs at synapses. We conclude that gephyrin exchange at synapses is tightly linked to GlyR stabilization.

This provides important insight into the dynamics of synaptic multimolecular assemblies in the control of synaptic strength.

Notably, β1 and β3 integrins affected inhibitory synaptic strength in an opposing fashion. β1 and β3 integrins have been shown to regulate other cell functions differentially. For example, L-type calcium channels are upregulated by β1 integrins and downregulated by β3 integrins in arteriolar smooth muscles for vasomodulation[31]. In macrophages, β1-mediated phagocytosis and migration (but not adhesion) are inhibited by β3 integrins[32]. This suggests that the functional counteraction between β1 and β3 integrins may be a general mechanism for adapting cellular responses to the extracellular environment. We sought to identify the molecular basis of the opposing actions of β1 and β3 integrins at glycinergic synapses and found that PKC was necessary for integrin effects inside and outside of synapses, consistent with the requirement of PKC for integrin activation[7]. We also found that CaMKII was responsible for β1 and β3 integrin actions specifically at synapses. CaMKII inhibition abolished the effects of integrin blockade at synapses, but not in the extrasynaptic membrane. Furthermore, CaMKII inhibition increased GlyR mobility at synapses and strongly decreased GlyR synaptic localization. These effects were similar to those observed after β1 integrin inhibition and β3 integrin activation with fibrinogen. Consistent with this, β1 and β3 integrins have been shown to activate and inhibit CaMKII, respectively[32]. Together, these data indicate that β1 and β3 integrins act via CaMKII to adjust GlyR trapping at synapses depending on the neuronal environment (**Supplementary Fig. 9**).

Our results suggest that CaMKII stabilizes GlyRs at inhibitory synapses. In contrast, CaMKII has been shown to destabilize PSD-95 at excitatory synapses[33] and to inhibit high-order complex formation between Homer and Shank *in vitro*[34]. This suggests that CaMKII regulates the dynamics of excitatory and inhibitory postsynaptic membranes in opposite directions to control neuronal activity. It will be important to identify the molecular targets of CaMKII for the regulation of inhibitory postsynaptic assembly dynamics. One possibility is that CaMKII directly targets gephyrin. Indeed, using *in vitro* phosphorylation tests and mass spectrometry, we found that CaMKII can phosphorylate gephyrin on at least six serine residues (**Supplementary Fig. 10**). Three of these sites have already been found to be phosphorylated *in vivo* (S296 (ref. 35), S318 (ref. 35), S337 (ref. 36)), suggesting that they are physiologically relevant. The sites that we identified are mainly located at the junction between the linker region and the C-terminal domain of gephyrin, which dimerizes and is essential for the formation of higher order oligomers (see refs. 29,37, and **Supplementary Fig. 10**). Further studies are required to determine whether β1 and β3 integrins modulate the phosphorylation state of these sites in living spinal cord neurons and how the multiple phosphorylation of gephyrin modulates its oligomerization properties.

Our results indicate that β1 and β3 integrins modulate inhibitory synapses in response to TSP1 or fibrinogen, two molecules that are released after injury[24–26]. TSP1 activates β1 integrins[23] and mediates neurite outgrowth and synaptogenesis for functional recovery[38]. In contrast, fibrinogen, a blood protein that is massively deposited in the spinal cord after injury, inhibits neurite outgrowth via β3 integrins[26]. Thus, in addition to their role in maintaining inhibitory synaptic strength under basal conditions, β1 and β3 integrins could modulate glycinergic inhibition in pathological and regenerative situations. These regulations may be crucial *in vivo* for the modulation of pain pathways[39,40] and spinal locomotor networks, which mainly rely on the proper equilibrium between glycinergic inhibition and glutamatergic excitation[41]. Notably, β3 integrins have been shown to regulate the numbers of AMPA receptors at excitatory synapses and are required for synaptic scaling in response to TNF-α[11]. This glia-dependent form of plasticity helps to adapt the activity of neuronal networks following chronic activity blockade or sensory deprivation[42,43]. Altogether, these data suggest that integrins orchestrate inhibitory and excitatory neurotransmission to adjust neuronal excitability in normal and pathological conditions.

METHODS

Methods and any associated references are available in the online version of the paper at http://www.nature.com/natureneuroscience/.

Note: Supplementary information is available on the Nature Neuroscience website.

ACKNOWLEDGMENTS

We thank members of the Triller laboratory, S. Supplisson, K. Aubrey, L. Wang and O. Pascual for kindly providing access to their patch-clamp rig and for helpful discussions, Y. Goda and L. Cingolani for integrin constructs and C. Specht, B. Barbour and R. Miles for critical reading of the manuscript. This work was supported by INSERM (A.T.), Agence Nationale de la Recherche (ANR08BLAN0282; A.T.), Fondation Pierre-Gilles de Gennes (A.T.), Institut pour la Recherche sur la Moelle épinière et l'Encéphale (A.T.), Ministère de la Recherche et de la Technologie (C.C. and P.M.) and Association Française contre les Myopathies (C.C.).

AUTHOR CONTRIBUTIONS

C.C. designed, performed and analyzed the experiments except for the *in vitro* phosphorylation assays and mass spectrometry and wrote the manuscript with help from the other authors. P.M. performed the *in vitro* phosphorylation assays. R.Y.T.-C. and D.R. performed mass spectrometry and analyzed data. I.M.M. supervised mass spectrometry and phosphorylation analyses. A.T. supervised the project.

COMPETING FINANCIAL INTERESTS

The authors declare no competing financial interests.

Published online at http://www.nature.com/natureneuroscience/.
Reprints and permissions information is available online at http://npg.nature.com/reprintsandpermissions/.

1. Triller, A. & Choquet, D. New concepts in synaptic biology derived from single-molecule imaging. *Neuron* **59**, 359–374 (2008).
2. Calamai, M. *et al.* Gephyrin oligomerization controls GlyR mobility and synaptic clustering. *J. Neurosci.* **29**, 7639–7648 (2009).
3. Gray, N.W., Weimer, R.M., Bureau, I. & Svoboda, K. Rapid redistribution of synaptic PSD-95 in the neocortex *in vivo*. *PLoS Biol.* **4**, e370 (2006).
4. Specht, C.G. & Triller, A. The dynamics of synaptic scaffolds. *Bioessays* **30**, 1062–1074 (2008).
5. Dahan, M. *et al.* Diffusion dynamics of glycine receptors revealed by single-quantum dot tracking. *Science* **302**, 442–445 (2003).
6. Hynes, R.O. Integrins: bidirectional, allosteric signaling machines. *Cell* **110**, 673–687 (2002).
7. Miranti, C.K. & Brugge, J.S. Sensing the environment: a historical perspective on integrin signal transduction. *Nat. Cell Biol.* **4**, E83–E90 (2002).
8. Pinkstaff, J.K., Detterich, J., Lynch, G. & Gall, C. Integrin subunit gene expression is regionally differentiated in adult brain. *J. Neurosci.* **19**, 1541–1556 (1999).
9. Chan, C.S., Weeber, E.J., Kurup, S., Sweatt, J.D. & Davis, R.L. Integrin requirement for hippocampal synaptic plasticity and spatial memory. *J. Neurosci.* **23**, 7107–7116 (2003).
10. Chavis, P. & Westbrook, G. Integrins mediate functional pre- and postsynaptic maturation at a hippocampal synapse. *Nature* **411**, 317–321 (2001).
11. Cingolani, L.A. *et al.* Activity-dependent regulation of synaptic AMPA receptor composition and abundance by beta3 integrins. *Neuron* **58**, 749–762 (2008).
12. Kloss, C.U. *et al.* Integrin family of cell adhesion molecules in the injured brain: regulation and cellular localization in the normal and regenerating mouse facial motor nucleus. *J. Comp. Neurol.* **411**, 162–178 (1999).
13. Staubli, U., Vanderklish, P. & Lynch, G. An inhibitor of integrin receptors blocks long-term potentiation. *Behav. Neural Biol.* **53**, 1–5 (1990).
14. Chan, C.S. *et al.* Beta 1-integrins are required for hippocampal AMPA receptor-dependent synaptic transmission, synaptic plasticity and working memory. *J. Neurosci.* **26**, 223–232 (2006).
15. Huang, Z. *et al.* Distinct roles of the beta 1-class integrins at the developing and the mature hippocampal excitatory synapse. *J. Neurosci.* **26**, 11208–11219 (2006).
16. Kramár, E.A., Lin, B., Rex, C.S., Gall, C.M. & Lynch, G. Integrin-driven actin polymerization consolidates long-term potentiation. *Proc. Natl. Acad. Sci. USA* **103**, 5579–5584 (2006).

17. Betz, H. & Laube, B. Glycine receptors: recent insights into their structural organization and functional diversity. *J. Neurochem.* **97**, 1600–1610 (2006).
18. Pfaff, M., McLane, M.A., Beviglia, L., Niewiarowski, S. & Timpl, R. Comparison of disintegrins with limited variation in the RGD loop in their binding to purified integrins alpha IIb beta 3, alpha V beta 3 and alpha 5 beta 1 and in cell adhesion inhibition. *Cell Adhes. Commun.* **2**, 491–501 (1994).
19. Wang, X.B. *et al.* Extracellular proteolysis by matrix metalloproteinase-9 drives dendritic spine enlargement and long-term potentiation coordinately. *Proc. Natl. Acad. Sci. USA* **105**, 19520–19525 (2008).
20. Charrier, C., Ehrensperger, M.V., Dahan, M., Levi, S. & Triller, A. Cytoskeleton regulation of glycine receptor number at synapses and diffusion in the plasma membrane. *J. Neurosci.* **26**, 8502–8511 (2006).
21. Lévi, S. *et al.* Homeostatic regulation of synaptic GlyR numbers driven by lateral diffusion. *Neuron* **59**, 261–273 (2008).
22. Hanus, C., Ehrensperger, M.V. & Triller, A. Activity-dependent movements of postsynaptic scaffolds at inhibitory synapses. *J. Neurosci.* **26**, 4586–4595 (2006).
23. DeFreitas, M.F. *et al.* Identification of integrin alpha 3 beta 1 as a neuronal thrombospondin receptor mediating neurite outgrowth. *Neuron* **15**, 333–343 (1995).
24. Möller, J.C. *et al.* Regulation of thrombospondin in the regenerating mouse facial motor nucleus. *Glia* **17**, 121–132 (1996).
25. Lin, T.N. *et al.* Differential regulation of thrombospondin-1 and thrombospondin-2 after focal cerebral ischemia/reperfusion. *Stroke* **34**, 177–186 (2003).
26. Schachtrup, C. *et al.* Fibrinogen inhibits neurite outgrowth via beta 3 integrin-mediated phosphorylation of the EGF receptor. *Proc. Natl. Acad. Sci. USA* **104**, 11814–11819 (2007).
27. Hanus, C., Vannier, C. & Triller, A. Intracellular association of glycine receptor with gephyrin increases its plasma membrane accumulation rate. *J. Neurosci.* **24**, 1119–1128 (2004).
28. Ehrensperger, M.V., Hanus, C., Vannier, C., Triller, A. & Dahan, M. Multiple association states between glycine receptors and gephyrin identified by SPT analysis. *Biophys. J.* **92**, 3706–3718 (2007).
29. Bedet, C. *et al.* Regulation of gephyrin assembly and glycine receptor synaptic stability. *J. Biol. Chem.* **281**, 30046–30056 (2006).
30. Zita, M.M. *et al.* Post-phosphorylation prolyl isomerisation of gephyrin represents a mechanism to modulate glycine receptors function. *EMBO J.* **26**, 1761–1771 (2007).
31. Wu, X. *et al.* Modulation of calcium current in arteriolar smooth muscle by alphav beta3 and alpha5 beta1 integrin ligands. *J. Cell Biol.* **143**, 241–252 (1998).
32. Blystone, S.D., Slater, S.E., Williams, M.P., Crow, M.T. & Brown, E.J. A molecular mechanism of integrin crosstalk: alphavbeta3 suppression of calcium/calmodulin-dependent protein kinase II regulates alpha5beta1 function. *J. Cell Biol.* **145**, 889–897 (1999).
33. Steiner, P. *et al.* Destabilization of the postsynaptic density by PSD-95 serine 73 phosphorylation inhibits spine growth and synaptic plasticity. *Neuron* **60**, 788–802 (2008).
34. Hayashi, M.K. *et al.* The postsynaptic density proteins Homer and Shank form a polymeric network structure. *Cell* **137**, 159–171 (2009).
35. Trinidad, J.C., Specht, C.G., Thalhammer, A., Schoepfer, R. & Burlingame, A.L. Comprehensive identification of phosphorylation sites in postsynaptic density preparations. *Mol. Cell. Proteomics* **5**, 914–922 (2006).
36. Tweedie-Cullen, R.Y., Reck, J.M. & Mansuy, I.M. Comprehensive mapping of post-translational modifications on synaptic, nuclear and histone proteins in the adult mouse brain. *J. Proteome Res.* **8**, 4966–4982 (2009).
37. Saiyed, T. *et al.* Molecular basis of gephyrin clustering at inhibitory synapses: role of G- and E-domain interactions. *J. Biol. Chem.* **282**, 5625–5632 (2007).
38. Liauw, J. *et al.* Thrombospondins 1 and 2 are necessary for synaptic plasticity and functional recovery after stroke. *J. Cereb. Blood Flow Metab.* **28**, 1722–1732 (2008).
39. Woolf, C.J. & Salter, M.W. Neuronal plasticity: increasing the gain in pain. *Science* **288**, 1765–1769 (2000).
40. Harvey, R.J. *et al.* GlyR alpha3: an essential target for spinal PGE2-mediated inflammatory pain sensitization. *Science* **304**, 884–887 (2004).
41. Grillner, S. The motor infrastructure: from ion channels to neuronal networks. *Nat. Rev. Neurosci.* **4**, 573–586 (2003).
42. Kaneko, M., Stellwagen, D., Malenka, R.C. & Stryker, M.P. Tumor necrosis factor–alpha mediates one component of competitive, experience-dependent plasticity in developing visual cortex. *Neuron* **58**, 673–680 (2008).
43. Stellwagen, D. & Malenka, R.C. Synaptic scaling mediated by glial TNF-alpha. *Nature* **440**, 1054–1059 (2006).

ONLINE METHODS

Primary neuronal culture. Primary cultures of spinal cord neurons were prepared from embryonic Sprague Dawley rats at day 14 as previously described[44] with a few modifications. Cells were plated at a density of 5×10^4 cells per cm^2. They were maintained in neurobasal medium supplemented with B27 (1×) and L-glutamine (2 mM) at 37 °C in 5% CO_2 for 11–14 d. The medium was changed every 4–5 d.

Constructs and transfection. Transfections were performed using Lipofectamine 2000 (Invitrogen). We used plasmids encoding with a gephyrin–Venus yellow fluorescent protein (VeGe[22]) fusion protein, EGFP, CTβ1 and CTβ3 (gift from Y. Goda, University College London)[11], and *c-myc*-α1βgb[45]. Cells were transfected 9 or 10 d after plating and imaged 48 h (VeGe) or 24 h (other constructs) later.

Cell treatment. We used monoclonal hamster antibody to rat β1 (aβ1, clone Ha2/5) and mouse antibody to rat β3 (aβ3, clone F11) to block integrin function (BD Pharmingen, 25 μg ml^{-1}). Blocking antibodies stabilize the inactive conformation of integrins[6]. Echistatin (100 nM), latrunculin A (3 μM), cycloheximide (100 μM) and leupeptin (100 μg ml^{-1}) were from Sigma. GRGDSP and GRGESP were from Bachem and used at 200 μM. Purified human platelet TSP1 was from either Sigma or Haematologic Technologies and used at 2 μg ml^{-1}. Purified human plasma fibrinogen (Calbiochem) was used at 1.5 mg ml^{-1} in 1.2 mM sodium citrate buffer. GF109203X/Bisindolylmaleimide I (Calbiochem) was used at 50 nM. KN-93 (10 μM), dynasore (80 μM), MG 132 (50 μM) and PP2 (10 μM) were from Tocris. Unless otherwise noted, cells were treated with aβ1, aβ3, echistatin, TSP1 or fibrinogen for 1 h before fixation or imaging. With the exception of cycloheximide (2 h), inhibitors were added 25 min before integrin-blocking antibodies. In live-cell imaging experiments, reagents were present in the recording medium.

Antibodies for immunodetection. α1-GlyRs were immunodetected using either a mouse antibody to α1-GlyR (mab2b, 0.7–1.25 μg ml^{-1}, Synaptic System) or a homemade rabbit antibody to α1-GlyR raised against the same extracellular epitope (1:800 to 1:1,500). No difference in GlyR lateral dynamics was observed with the mouse and rabbit primary antibodies[21]. We also used mouse antibody to gephyrin (mAb7a, 1.25 μg ml^{-1}, Synaptic System), rabbit antibody to gephyrin (homemade, 1:1,000), 9E10 (Millipore) and rabbit antibody to synapsin I (1.7 μg ml^{-1}, Synaptic System). For secondary antibodies, we used Cy3-conjugated goat antibody to mouse (1.25 μg ml^{-1}), Cy3-conjugated goat antibody to rabbit (2.5 μg ml^{-1}) and Alexa 488–conjugated goat antibody to rabbit (2.5 μg ml^{-1}). Secondary antibodies used in SPT were biotinylated Fab fragments (goat antibody to mouse, 1 μg ml^{-1}; goat antibody to rabbit, 2 μg ml^{-1}). All secondary antibodies were from Jackson ImmunoResearch, except for the Alexa 488–conjugated antibody, which was from Invitrogen.

Immunocytochemistry, image acquisition and quantitative analysis. Immunocytochemistry, image acquisition and fluorescence quantification were performed as previously described[20]. The images shown in **Supplementary Figure 2** were obtained using a Leica DM5000B microscope equipped with a Yokogawa CSU 10 spinning disk. Sets of neurons compared with quantification were fixed, labeled and imaged in parallel. Analyses were performed using MetaMorph (MetaImaging). GlyR and gephyrin synaptic amounts were quantified in double-labeling experiments by measuring the fluorescence intensity associated with GlyR or gephyrin clusters apposed to presynaptic terminals labeled with synapsin I. In our dissociated spinal cord neurons, 90% of GlyR and gephyrin clusters were apposed to presynaptic terminals[46]. Thus, all GlyR and gephyrin clusters were analyzed when cells were treated with aβ1 and aβ3. The effects of aβ1 and aβ3 on GlyR cluster immunoreactivity were examined in nonpermeabilized neurons. A procedure based on wavelet decomposition was used to quantify synapse density and synapse size[22].

Single particle imaging. Cells were labeled and imaged in MEM recording medium consisting of MEM (Invitrogen) supplemented with 10 mM HEPES, 33 mM glucose, 2 mM glutamine, 1 mM sodium pyruvate and B27 at 37 °C. Cells were incubated for 5 min with primary antibodies, washed, incubated for 5 min with biotinylated secondary Fab and washed again. Cells were then incubated for 1 min with streptavidin-coated quantum dots emitting at 605 nm (1 nM, Invitrogen) in borate buffer (50 mM). After extensive washing, active presynaptic terminals were stained for 40 s with FM4-64 (3 μM, Invitrogen) in the presence of 40 mM KCl. Cells were imaged in an open chamber mounted on an inverted microscope (IX71, 60× objective, NA = 1.45, Olympus). Quantum dots and FM4-64 were detected using a Hg^+ lamp and appropriate filters (quantum dot: D455/70x, HQ605/20m; FM4-64: D535/50x, E590lpv2; Chroma Technology). Quantum dots were recorded for 512 consecutive frames at 13 Hz with a CCD camera (Cascade 512BFT; Roper Scientific) and MetaView (MetaImaging). Cells were imaged 30 min after labeling.

SPT and quantitative analysis of lateral diffusion. Analyses were restricted to single quantum dots identified by the intermittency of their fluorescence. Synapses were identified from FM4-64 images using a procedure based on wavelet decomposition[22]. SPT was performed using custom software written with MATLAB (MathWorks)[28]. Quantum dot localization was determined with a spatial accuracy of about 10 nm by cross-correlating the image with a Gaussian model of the point spread function and GlyR-QD trajectories were reconstructed as previously detailed[28].

Diffusion coefficients were calculated from the longest fragment of the trajectory spent in the synaptic and extrasynaptic compartment, determined by comparison of the trajectories with the FM4-64 image. Only fragments longer than 30 consecutive frames were taken into account. The MSD was calculated using

$$\mathrm{MSD}(ndt) = (N - n)^{-1} \sum_{i=1}^{N-n} ((x_{i+n} - x_i)^2 + (y_{i+n} - y_i)^2) dt,$$

where x_i and y_i are the coordinates of an object on frame i, N is the total number of steps in the trajectory, dt is the time interval between two successive frames, and ndt is the time interval over which displacement is averaged[47]. Diffusion coefficients were calculated with a fit between data points 2 and 5 of the MSD curves versus time (t) as previously described[28]. Distributions, rather than mean values, were compared because of the large dispersal of the values (over four orders of magnitude). Diffusion parameters could vary from one culture another, imposing comparisons with internal controls. Diffusion coefficients at synapses were compared in the 25–75% interquartile range. To evaluate the effects of aβ1 and aβ3 treatments, we divided the distributions into ten classes with an equal number of values, and the mean diffusion coefficient was calculated for each class. Ratios of the means in aβ1 and aβ3 conditions over the means in control were used as an indicator of aβ1 and aβ3 effects.

Confined trajectories were determined according to the relative deviation of the experimental MSD with the one expected in the case of Brownian diffusion (adapted from ref. 48). The size of the confinement domain for trajectories showing restricted motion was calculated as previously described[28].

The time spent by single GlyR-QDs in the synaptic and extrasynaptic compartments and the number of transitions between the two compartments were determined as previously described[20]. For GlyR-QDs transiting between the synaptic and extrasynaptic compartments, dwell time index = time spent at synapses / (total time detection × n exits from synapses). For GlyR-QDs always detected at synapses, dwell time index = 1. Only GlyR-QDs with a dwell time index > 0.03 were taken into account.

Fluorescence recovery after photobleaching. Experiments were performed at 37 °C in MEM recording medium. Active synapses were stained with FM 4-64 as described above. Cells were observed on an inverted microscope (Eclipse TE2000-E, 100× objective, NA = 1.4, Nikon) equipped with a DG-4 illumination system (Sutter Instruments) and appropriate filter sets (Semrock, Optoprim), a CCD camera (QuantEM 512SC, Roper Scientific) and a FRAP-3D system (Roper Scientific). The procedure was controlled with MetaMorph. Fluorescence was photobleached using a 488-nm laser at 65 mW for 80 ms in 3–4 regions of interest (diameter, 1–1.2 μm) centered on individual VeGe synaptic clusters. Photobleaching in the 3–4 regions of interest was quasi-simultaneous. Fluorescence was monitored in time-lapse. Three images were acquired before the photobleaching within a period of 1 min. The recovery after photobleaching was monitored as follows: 1 image every 10 s for 5 min, 1 image every 20 s for 5 min and 1 image every 60 s for 10 min. At each time point, three images were acquired in z stack with a step size of 0.4 μm. Data were analyzed from maximum intensity projection using MetaMorph.

Fluorescence recovery was measured after background subtraction and correction for the ongoing photobleaching as follows: $Fcorr_t = (F_t/F_0)/(Fnb_t/Fnb_0)$, where F_t is the fluorescence at time t, F_0 is the mean fluorescence before bleaching, Fnb_t is the average fluorescence intensity of three nonbleached spots at time t, and Fnb_0 is the average fluorescence intensity of the same nonbleached spots before bleaching.

Electrophysiology. Whole-cell patch-clamp recordings were performed using a multiclamp 700B controlled by Clampex 10 (Axon Instruments). Patch-pipettes had a tip resistance of 3.5–5 MΩ when filled with an intracellular solution containing 68 mM potassium glutamate, 68 mM KCl, 0.2 mM EGTA, 2 mM $MgSO_4$, 20 mM HEPES buffer, 3 mM Na_2ATP and 0.2 mM Na_3GTP. The external solution contained 136 mM NaCl, 2.5 mM KCl, 2 mM $CaCl_2$, 1.3 mM $MgCl_2$, 10 mM HEPES and 10 mM D-glucose. It was supplemented with 1 µM TTX, 50 µM D-AP5, 2 µM NBQX and 5 µM gabazine (SR95531) to isolate glycinergic mIPSC. All the supplements were from Tocris. About 10 min after mIPSC isolation, aβ1 or aβ3 (20 µg ml^{-1}) was added to the external solution for 5 min (flow ≈1 ml/min) to allow the immunoreaction. mIPSCs were recorded at a holding potential of −60 mV at 30 °C. Recordings were filtered at 4 kHz and sampled at 20 kHz using a Digidata 1440A (Axon Instruments). Throughout the experiment, the access resistance was tested periodically and cells were discarded if the access resistance changed by more than 15% or was more than 20 MΩ. mIPSCs were detected using the template procedure of the Clampfit 10 program (Axon Instruments) and analyzed over 2-min periods. mIPSCs recorded 15 min after treatment with antibodies were compared with mIPSCs before application. In control cells, mIPSCs from 2-min periods separated by 20 min were compared. All cells with mean mIPSC frequency higher than 1 Hz were taken into account.

Cell surface biotinylation, quantification of GlyR and gephyrin levels. After 1 h treatment with aβ1 or aβ3, cells were washed three times with ice-cold Dulbecco's phosphate-buffered saline (DPBS) supplemented with 0.8 mM $CaCl_2$ and 0.5 mM $MgCl_2$, pH 7.4 ($DPBS^{2+}$). They were then incubated twice with biotinylation reagent (1 mg ml^{-1} NHS-SS-biotin, Pierce) for 12 min with gentle shaking on ice. Cells were then washed and unbound biotin was quenched with 50 mM glycine in $DPBS^{2+}$/BSA for 15 min. Cell extracts were collected by scraping the cells in a Tris buffer consisting of 50 mM Tris-HCl (pH = 8), 100 mM NaCl, 1 mM PMSF (Sigma) and a protease inhibitor cocktail (Roche). Neurons were lysed with 3% Triton X-100 (wt/vol) in Tris buffer supplemented with 2 mM EDTA for 1 h on ice. Cleared Triton extracts were collected after centrifugation for 15 min at 10,000*g*. The blocking antibodies were removed by incubation with protein G immobilized on sepharose (Sigma) in Tris buffer supplemented with 1% Triton X-100 and 2 mM EDTA (binding buffer) for 1 h at 4 °C. The blocking antibodies were not detected with western blot following this procedure. We collected 20% of the sample as the total receptor fraction. The remaining 80% was mixed with neutravidin beads (Pierce) for 2 h at 4 °C to purify the biotinylated proteins (surface proteins). Proteins were separated and analyzed by SDS-PAGE followed by immunoblotting with mAb4a antibody (Synaptic System, 1:600), rabbit antibody to GluR2 (Millipore, 1:200), rabbit antibody to GAPDH (Abcam, 1:2,000) and rabbit antibody to gephyrin (Santa Cruz, 1:1,500). Proteins were visualized with enhanced chemiluminescence (ECL+, Amersham). The level of surface receptor was normalized to the corresponding level of total receptor detected. The level of total receptor or gephyrin was normalized to the corresponding level of GAPDH.

***In vitro* phosphorylation assay.** The Ge(4′) gephyrin isoform was used to address gephyrin phosphorylation by CaMKII *in vitro*. This gephyrin isoform was cloned from the rat spinal cord[49]. It is specifically expressed in the CNS[50] and it binds to the GlyR. The C4′ cassette of gephyrin does not interfere with GlyR/gephyrin binding *in vitro*[49], but it contains a consensus site for phosphorylation by CaMKII. Recombinant Ge(4′) has been described previously (Ge(2,4′), see ref. 29). Gephyrin was expressed in transformed *E. coli* and purified under native conditions by nickel-nitrilotriacetic acid (Ni-NTA) affinity chromatography as described previously[29]. Recombinant CaMKIIα (Cell Signaling Technology) and GST-CaMKIIβ fusion protein (Sigma) were pre-incubated for 10 min at 30 °C in kinase buffer (50 mM Tris-HCl (pH 7.5), 10 mM $MgCl_2$, 2 mM DTT, 0.1 mM Na_2EDTA, 200 µM ATP, 10 mM NaF, 2 mM Na_3VO_4 and 5 mM $Na_4P_2O_7$.H2O) supplemented with 2 mM $CaCl_2$ and 1.2 µM calmodulin. In control experiments, CaMKII was pre-incubated in the absence of $CaCl_2$ and calmodulin (inactive CaMKII). Recombinant gephyrin Ge(4′) was incubated in kinase buffer with activated or inactive CaMKII for 30 min at 30 °C. The reaction was stopped by heating at 65 °C for 20 min. CaMKII activity was verified using the highly selective CaMKII substrate autocamtide-2 (Sigma).

Mass spectrometry. Gephyrin (2 µg) bound to Ni-NTA agarose beads were reduced with 2 mM dithiothreitol for 60 min and alkylated with 4.2 mM iodoacetamide for 1 h at 21 °C. We added 100 µl of 100 mM ammonium bicarbonate (pH 7.8) and 13 µl methanol to the samples and adjusted the pH to 7.8. Samples were heated for 15 min at 60 °C before the addition of trypsin (enzyme to substrate, 1:150). Samples were digested for 3 h at 37 °C and the reaction stopped by the addition of trifluoroacetic acid (TFA) then lyophilized to remove methanol. Autocamtide-2 samples were treated in the same manner.

Titanium oxide and immobilized metal affinity chromatography pipettes were used for enriching phosphopeptides from the digests. MonoTip TiO pipettes were prepared as per manufacturer's instructions (GL Sciences). Phosphopeptides were bound and washed as previously described[36] and then eluted twice with 150 µl 0.3 M ammonium hydroxide solution. Unbound peptides were lyophilized and resuspended in 100 µl of binding solution (10% acetonitrile (ACN), 0.1% acetic acid). ZipTip 10 µl Metal Chelator pipette tips (Waters) were prepared and the residual phosphopeptides bound and washed as per manufacturer's instructions (Waters). All phosphopeptide-enriched samples were quickly lowered to pH = 3 using TFA and then cleaned with ZipTip C18 tips (Waters) before mass spectrometry analysis.

Samples were analyzed on a calibrated hybrid LTQ Orbitrap XL electron transfer dissociation (ETD) mass spectrometer (Thermo Scientific). Peptides were resuspended in 3% ACN (vol/vol) and 0.2% formic acid and loaded on a 10 cm fused silica column packed with 3 µm 200 Å pore size C18 resin. Peptides were eluted via an ACN gradient of 5–30% ACN over 35 min and 30–80% ACN over the subsequent 13 min in a buffer containing of 0.2% formic acid at flow rate of 200 nl min^{-1}. One scan cycle comprised of a full-scan mass spectrometry survey spectrum from m/z 300–2,000 acquired in the FT-Orbitrap, followed by up to six sequential collision-induced dissociation (CID) and ETD mass spectrometry/mass spectrometry scans with fragment ion detection in the linear ion trap. CID was performed with a target value of 1e4 in the linear trap, collision energy at 35%, Q value at 0.25 and activation time at 30 ms. AGC target values were 5×10^5 for full FTMS scans and 1×10^4 for ion trap MSn scans. The ETD anion target value was set at 1e6 and activation time at 100 ms. Supplementary activation was employed to enhance the fragmentation efficiency for bi-cationic precursors and charge state–dependent ETD time was enabled. A Data dependent decision tree was used to control ETD dissociation based on charge and m/z. The ETD reaction time was 120 ms and isolation width was 2 m/z. For all experiments, dynamic exclusion was used with 1 repeat count, 30-s repeat duration and 10-s exclusion duration. Samples were acquired using internal lock mass calibration set on m/z 429.088735 and 445.120025.

Mass spectrometry and mass spectrometry/mass spectrometry data were processed with Mascot distiller and searched using Mascot version 2.2. The Monoisotopic masses of 2+ or greater charged peptides were searched with a peptide tolerance of 8 ppm and an MS/MS tolerance of 0.6 Da for fragment ions using a rat protein database downloaded from the European Bioinformatic Institute. Modifications used for searches included carbamidomethyl (C, variable) and phosphorylation (STY, variable). Only strictly tryptic peptides with a maximum of 4 missed cleavage sites were allowed. Positive identification of phosphorylated peptides was performed using a variety of strict criteria. Only bold-red, rank 1 peptides with Mascot expect values of less than 0.05 were considered and then manually evaluated for precise site assignment as previously described[36].

Statistics. Data were obtained from at least three independent experiments, except when aβ1 and aβ3 effects were tested after another treatment (two independent experiments). Statistical analyses were performed with StatView (Abacus Concept) or R. Differences in diffusion coefficients, confinement domain size, dwell time index, FRAP and mIPSCs were assessed using the Mann-Whitney test. Data obtained with immunocytochemistry were compared using the unpaired two-tailed Student's *t* test. Multiple comparisons

doi:10.1038/nn.2645

of mean effects on diffusion coefficients, mIPSC amplitudes and mIPSC frequency were performed using ANOVA followed by the least significant difference post-hoc test. Normality of the distributions was determined using the one-sample Kolmogorov-Smirnov test. A test was considered significant when $P < 0.05$. Data are expressed as mean ± s.e.m.

44. Lévi, S., Vannier, C. & Triller, A. Strychnine-sensitive stabilization of postsynaptic glycine receptor clusters. *J. Cell Sci.* **111**, 335–345 (1998).
45. Meier, J., Meunier-Durmort, C., Forest, C., Triller, A. & Vannier, C. Formation of glycine receptor clusters and their accumulation at synapses. *J. Cell Sci.* **113**, 2783–2795 (2000).
46. Dumoulin, A., Levi, S., Riveau, B., Gasnier, B. & Triller, A. Formation of mixed glycine and GABAergic synapses in cultured spinal cord neurons. *Eur. J. Neurosci.* **12**, 3883–3892 (2000).
47. Saxton, M.J. Single-particle tracking: the distribution of diffusion coefficients. *Biophys. J.* **72**, 1744–1753 (1997).
48. Kusumi, A., Sako, Y. & Yamamoto, M. Confined lateral diffusion of membrane receptors as studied by single particle tracking (nanovid microscopy). Effects of calcium-induced differentiation in cultured epithelial cells. *Biophys. J.* **65**, 2021–2040 (1993).
49. Meier, J., De Chaldee, M., Triller, A. & Vannier, C. Functional heterogeneity of gephyrins. *Mol. Cell. Neurosci.* **16**, 566–577 (2000).
50. Paarmann, I., Schmitt, B., Meyer, B., Karas, M. & Betz, H. Mass spectrometric analysis of glycine receptor-associated gephyrin splice variants. *J. Biol. Chem.* **281**, 34918–34925 (2006).